EPJ B
Condensed Matter and Complex Systems
EPJ.org
your physics journal

Eur. Phys. J. B (2017) 90: 18 DOI: 10.1140/epjb/e2016-70637-9

A comparative study of threshold effects in the energy loss moments of protons, electrons and positrons using dielectric models for band-gap materials

Claudio Darıo Archubi and Nestor R. Arista

edp sciences
Società Italiana di Fisica
Springer

Eur. Phys. J. B (2017) 90: 18
DOI: 10.1140/epjb/e2016-70637-9

THE EUROPEAN PHYSICAL JOURNAL B

Regular Article

A comparative study of threshold effects in the energy loss moments of protons, electrons and positrons using dielectric models for band-gap materials

Claudio Darıo Archubi[1,a] and Nestor R. Arista[2]

[1] Instituto de Astronomía y Física del Espacio-UBA-Conicet, Ciudad Universitaria, 1428 Buenos Aires, Argentina
[2] División Colisiones Atómicas, Centro Atómico Bariloche and Instituto Balseiro, 8400 S.C. Bariloche, Argentina

Received 27 October 2016 / Received in final form 1st December 2016
Published online 25 January 2017 –

Abstract. A comparative study of the energy loss, mean free path and straggling of protons, positrons and electrons in an electron gas is performed using three dielectric models which represent the case of metals (Lindhard model for a free electron gas) and the cases of semiconductors and insulators (Levine and Louie model and Brandt and Reinheimer model for systems with a band gap). The properties of individual and collective contributions according to each model and for each of the particles are analyzed. In particular, the effects produced by the band gap of the material and by the properties of the incident particle are analyzed in detail. Significant differences related to the mass and to the indistinguishability (in the case of electrons) are described. Analytical expressions for the high-energy limit are derived in a simple way using the plasmon-pole approximation.

1 Introduction

The interaction of light ions with solids is one of the most powerful tools to study and modify the properties of different materials, and yields access to many techniques and applications. This includes several topics related to applied physics, medical treatments, space and materials science, and others. The recent advances in the areas of nanotechnology and electronic devices provide new stages for scientific research and applications that involve the interaction of light ions with materials with different electronic and structural properties. It is in the context of the advances in these new areas that detailed studies and quantitative comparisons between the interactions produced by different types of particles on material with different electronic properties is of great current interest.

Several studies of stopping powers and mean-free-paths of electrons in solids have already been made, starting with the pioneering work by Ashley et al. for metallic elements [1], and further studies by Akkerman et al for insulating materials [2], as well as a set of very complete calculations of inelastic scattering of electrons and positrons in a free electron gas by Fernández-Varea et al. [3]. A recent review of electron attenuation lengths in solids may be useful for further references in this area [4].

However, to our knowledge, no systematic comparisons between protons, electrons and positrons, using different dielectric models appropriate for band-gap materials have been made. The cases of interest include in particular different types of insulators or compounds with large band gaps, which are some of the basic materials of current interest for many of the applications mentioned before.

Based on these premises we aim here to describe and compare in detail the characteristics of the interactions between electrons, positrons and protons, with a material characterized in terms of different dielectric approaches, including in particular three main models [5–8] that represent the cases of metals (free electron gas) [5], semiconductors, and insulators (systems with a band gap) [6–8]. As part of this study we describe the appearance and the characteristics of threshold effects in the interaction of electrons, positrons and protons with those materials. For this study, three representative parameters are considered: the stopping power, the mean-free path, and the energy straggling, showing the differences that arise in all these cases.

The present work is organized as follows: in Section 2 we describe the dielectric approaches used in this study including the expressions for the various energy loss moments that can be applied to the three particles considered in this study. In Section 3 we show the calculations of the energy loss moments for protons, positrons and electrons, showing and comparing the contributions due to individual and collective excitations, and comparing the results for the three types of particles. The conclusions are summarized in Section 4. We also include an Appendix where the method of line integral for the plasmon term and the plasmon-pole approximations are reviewed and useful

[a] e-mail: archubi@iafe.uba.ar

analytical expressions for the high-energy limit of the energy-loss moments are derived.

2 Dielectric models

We shall compare the first three moments of the energy distribution for protons, electrons and positrons traversing an electron gas with $r_s = 1.5$, without a band gap, and with a band gap $E_g = 14$ eV. For this purpose we shall use the same approaches that have been used in reference [9] for the case of protons, namely: the full-scale formulation involved in Brandt-Reinheimer dielectric model [6,7] and the heuristic approach of Levine-Louie dielectric model [8]. To analyze the effects of the energy gap more closely the results of these models will be compared with those of a free electron gas using Lindhard's model [5,10].

For all these cases, the dielectric function of the material is expressed in terms of reduced variables in the following way (see Ref. [9] for further details):

$$\varepsilon(k,\omega) = 1 + g(z,E_g)[f_1(z,u,E_g) + if_2(z,u,E_g)] \quad (1)$$

where k and ω represent the momentum and energy transfers to the medium, and u and z are the corresponding reduced variables defined by the relations: $z = k/2k_F$, $u = \omega/kv_F$. E_g is the energy gap of the material ($E_g = 0$ for Lindhard dielectric function), and v_F and E_F are the Fermi velocity and corresponding energy. Other important quantities to characterize the system are the electron density n, the plasma frequency $\omega_p = (4\pi ne^2/m)^{1/2}$ and the electronic Wigner-Seitz radius $r_s = 1.919/v_F$.

The first-order moment of the energy-loss distribution yields the mean energy loss, or *stopping power*, calculated in the dielectric formulation by the integral expression [11]:

$$\frac{dE}{dx} = \frac{2}{\pi}\frac{e^2}{v^2}\int_0^{k_{\max}} \frac{dk}{k}(1 + f_{ex}(k)) \times \int_0^{\varpi_{\max}} \omega d\omega \ \mathrm{Im}\left[\frac{-1}{\varepsilon(k,\omega)}\right]. \quad (2)$$

Several important differences exist between this expression and that considered in reference [9] for the case of protons. First, the exchange term: $f_{ex}(k) = (\hbar k/mv)^4 - (\hbar k/mv)^2$ for electrons, and $f_{ex}(k) = 1$ for positrons, takes into account the exchange effects in the electron-electron interaction due to the indistinguishability of scattered and ejected electrons when the energies of both electrons are similar. Second, we cannot neglect the quadratic term in the maximum transferred energy $\varpi_{\max} = kv - \frac{\hbar k^2}{2m}$ (recoil effect) by an electron or positron with incident energy $T = mv^2/2$. Third, the Pauli exclusion principle is taken into account setting the condition that $\hbar\varpi_{\max}$cannot exceed the value $T - (E_g + E_F)$. Finally, another additional condition is necessary for the special case of electrons: the indistinguishability between the incident and the ejected electron requires that the maximum energy transfer cannot exceed $T/2$ [11].

The zero-order moment, or *inverse mean free path*, is obtained from the expression:

$$\lambda^{-1} = \frac{2}{\pi}\frac{e^2}{\hbar v^2}\int_0^{k_{\max}} \frac{dk}{k}(1 + f_{ex}(k)) \times \int_0^{\varpi_{\max}} d\omega \ \mathrm{Im}\left[\frac{-1}{\varepsilon(k,\omega)}\right]. \quad (3)$$

The second-order moment or *straggling*, associated to the dispersion in the energy loss, is calculated as:

$$\Omega^2/dx = \frac{2}{\pi}\frac{\hbar e^2}{v^2}\int_0^{k_{\max}} \frac{dk}{k}(1 + f_{ex}(k)) \times \int_0^{\varpi_{\max}} \omega^2 d\omega \mathrm{Im}\left[\frac{-1}{\varepsilon(k,\omega)}\right]. \quad (4)$$

All the moments $i = 0, 1, 2$ can be characterized by a dimensionless number L^i separated into two contributions: $L^i = L^i_{eh} + L^i_{pl}$, corresponding to the excitation of single individual electrons, or electron-hole pairs (L^i_{eh}), and collective or plasmon excitations (L^i_{pl}), as explained in reference [9]. The calculation of the eh term is made by integrating equations (2)–(4) over the region of the $k - \omega$ plane where the imaginary part of $\varepsilon(k,\omega)$ is different from zero, while the calculation of the plasmon component requires a different procedure; in this case the integral can be transformed into a line integral along the resonance line corresponding to the plasmon dispersion curve defined by $\varepsilon(k,\omega) = 0$. This procedure is described in detail in the Appendix.

In the following we present a set of calculations of the three relevant energy-loss moments mentioned before, considering a material described by $r_s = 1.5$, and energy gap values $E_g = 0$ and $E_g = 14$ eV. The case with $r_s = 1.5$ and $E_g = 14$ eV corresponds to the particular case of LiF; however similar properties may be expected for other insulators such as Al_2O_3 ($r_s = 1.5$, $E_g = 8$ eV), AlF_3 ($r_s = 1.446$, $E_g = 10.8$ eV), NaCl ($r_s = 2.088$, $E_g = 8.5$ eV). Other cases of interest include semiconductors, such as Si and Ge, with r_s values close to 2 but much smaller energy gaps, so that threshold effects will be strongly reduced (see Ref. [9]).

3 Calculations of energy loss moments

3.1 Protons

In Figures 1a and 1b we show some illustrative results for all the moments calculated using the three dielectric models considered here (Lindhard, Levine-Louie and Brandt-Reinheimer) in the case of protons traversing an electron gas characterized by $r_s = 1.5$. In panel (1) of Figure 1a we show stopping calculations, separating the contributions of electron-hole (eh) and plasmon (pl). For the Lindhard case, three main aspects of the energy loss phenomenon may be noticed: panel (1) of Figure 1a shows the proportionality with ion speed in the low energy range,

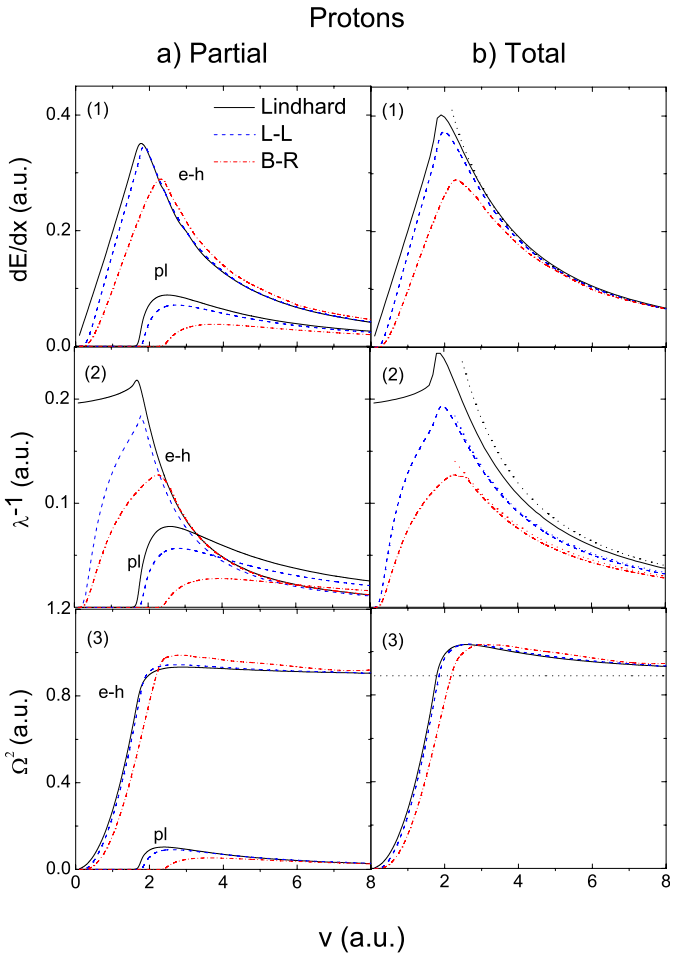

Fig. 1. (a) Separate contributions from individual and collective excitations to the energy-loss moments versus the projectile velocity for a proton impinging on a medium represented by a free electron gas with $r_s = 1.5$ a.u. Comparisons between the three dielectric models: full-line, Lindhard model (energy gap = 0 eV), dashed-line, Levine-Louie model (energy gap = 14 eV), dashed-dotted line, Brandt-Reinheimer model (energy gap = 14 eV). (Panel 1) Stopping power vs. projectile velocity. (Panel 2) Inverse mean free path vs projectile velocity. (Panel 3) Straggling vs. projectile velocity. (b) Total contributions (individual+collective excitations) dotted line, high energy limit.

where only *eh* excitations can take place, and the threshold for plasmon excitation, in the region around the stopping power maximum; panel (1) of Figure 1b shows the total stopping power, and its convergence to the Bethe limit at high energies, i.e. [6,7]

$$\left.\frac{dE}{dx}\right|_{Bethe} = \frac{e^2\omega_p^2}{v^2}\ln\left(\frac{\alpha_1 m v^2}{\hbar\overline{\omega}_p}\right) \tag{5}$$

where $\overline{\omega}_p = \left[\omega_p^2 + E_g^2/\hbar^2\right]^{1/2}$, and $\alpha_1 = 2$ for protons. Notice that when $E_g = 14$ eV the stopping curve at low speeds deviates from the linear dependence corresponding to a free electron gas. This "threshold effect", is a consequence of the energy gap and has been analyzed in reference [9].

In panel (2) of Figure 1a we show similar calculations for the mean free path. Here we notice that at low speeds there is a significant deviation from the behavior corresponding to a free electron gas. This effect is even more interesting than the one obtained for the stopping because it could be easier to be detected in the experiments. Panel (2) of Figure 1b shows that at high energies the total results for protons converge to the following limit (see Appendix for further details)

$$\lambda^{-1}\big|_{Bethe} = \frac{e^2\omega_p^2}{v^2}\frac{1}{\hbar\overline{\omega}_p}\ln\left(\alpha_0\frac{v}{v_F}\right) \tag{6}$$

where α_0 is a numerical constant that depends on the dielectric model.

In panel (3) of Figure 1a similar results are shown for the straggling term. As shown in this figure the plasmon contribution to the straggling is small. Notice that there is also a shift between the results for a free electron gas and the results with an energy gap. However, due to the more pronounced dependence of the straggling with velocity in the low-energy region, and additional difficulties to measure al low energies [12], it would be more difficult to detect this shift in the experiments. In panel (3) of Figure 1b the results are compared with Bohr's limit, corresponding to binary collisions at high speeds. In this limit, the total straggling per unit length is approximated by:

$$\Omega^2/dx\big|_{Bohr} = 4\pi n e^4\alpha_2 \tag{7}$$

where n is the electron density and $\alpha_2 = 1$ for protons. The figure shows also a notorious "overshooting" of the calculated straggling with respect to the Bohr value. This effect has been predicted theoretically and experimentally observed [13].

3.2 Positrons

In Figures 2a and 2b we show the results for all the moments calculated using the three dielectric models in the case of positrons traversing an electron gas characterized by $r_s = 1.5$. Figure 2a shows the contributions of electron-hole and plasmons for the three dielectric models. Figure 2b shows the corresponding total values. In panel (1) of Figure 2a we observe for low velocities a nonlinear dependence of the stopping as a function of the projectile velocity v, even for a free electron gas, as predicted by Ritchie [14]. The energy gap produces an additional shift of the curve for both contributions (*eh* and *pl*) in the region of low velocities, but the nonlinear dependence makes it more difficult to observe this threshold effect experimentally than in the case of protons. The results shown in panel (2) of Figure 2a suggest that the threshold effect due to the energy gap could be detected more easily in the experiments if the mean free path is measured. Finally, we notice that the relative contributions of plasmons is higher for positrons than for protons. The importance of the plasmon contribution produces a sudden change

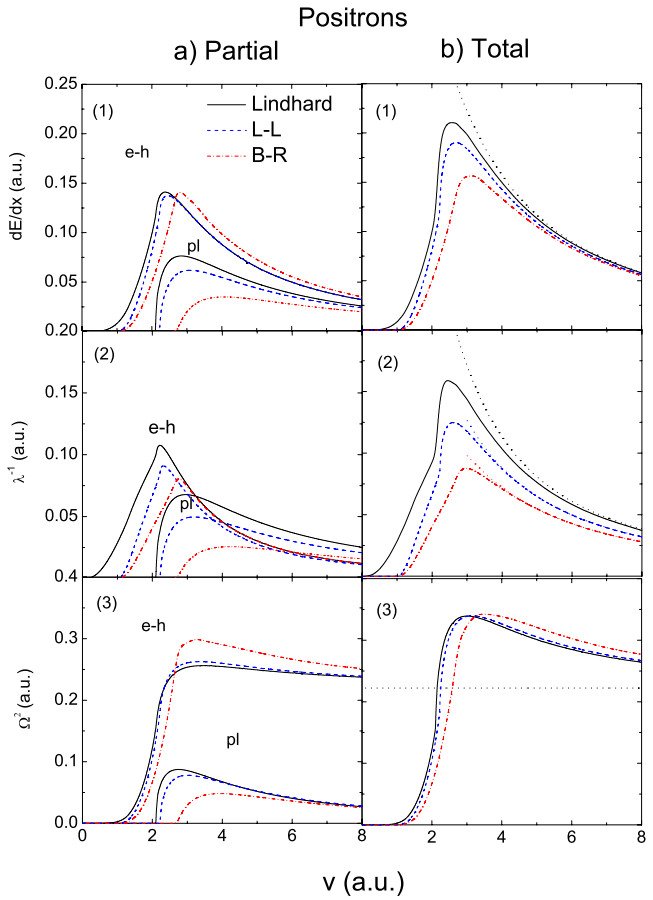

Fig. 2. Similar conditions to Figure 1 for a positron impinging on a medium represented by a free electron gas with $r_s = 1.5$ a.u.

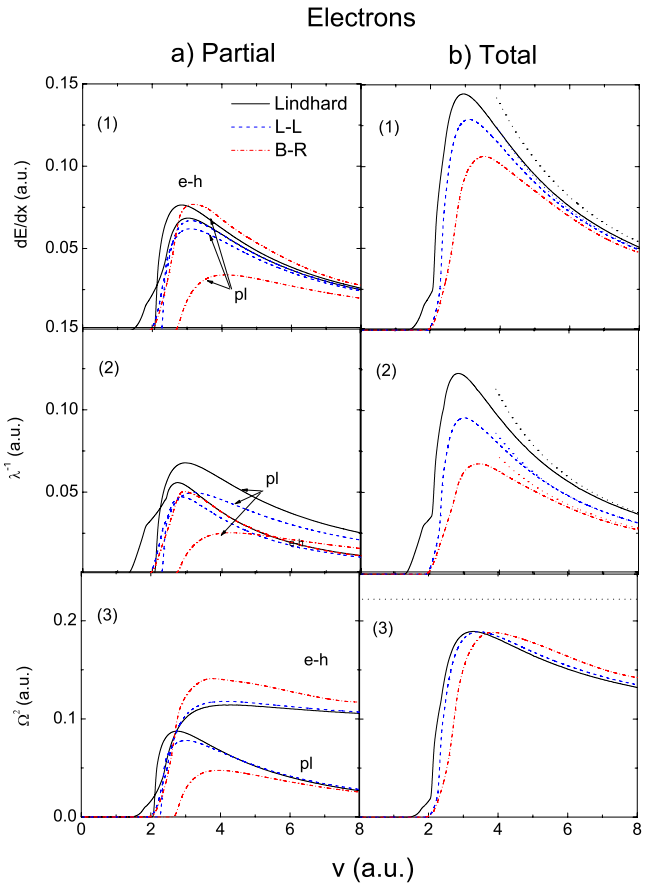

Fig. 3. Similar conditions to Figure 1 for an electron impinging on a medium represented by a free electron gas with $r_s = 1.5$ a.u.

of slope in the cases of Lindhard and Levine-Louie for the total results, as is shown in all the panels of Figure 2b. The high-energy limits from the equations derived in the Appendix are also shown in Figure 2b, where $\alpha_{1,2} = 1, 0.25$ for the stopping and straggling respectively, and $\alpha_0 = 1.6, 1.05, 0.8$ for the inverse mean-free path of positrons, for the Lindhard, Levine-Louie and Brandt-Reinheimer models, respectively.

3.3 Electrons

In Figures 3a and 3b we show the results for all the moments calculated using the three dielectric models in the case of electrons traversing an electron gas characterized by $r_s = 1.5$. In Figure 3a, we observe that the energy gap also produces a large shift of all the curves for low velocities. The expected presence of a threshold effect is explained by similar reasons to those exposed in the analysis of the results for protons and positrons, with the additional restrictions imposed by the Pauli principle. Notice also that panels (1) and (2) of Figure 3a show a sudden change in the slope of the e-h stopping and inverse mean free path curves for the case of Lindhard dielectric model at low energies. This behavior is not present for positrons and it is produced by the additional restrictions to the maximum transferred energy when the projectile is an electron. However, the presence of a wide energy gap eliminates this anomaly as it can be appreciated in panels (1) and (2) of Figure 3a for the cases of Levine-Louie and Brandt-Reinheimer dielectric models. Figure 3b shows that this behavior is present also in the total results for the case of Lindhard model. The high-energy limits of equations (5), (6), (7) are also shown in Figure 3b, where $\alpha_1 = 0.7$ for the stopping term, $\alpha_2 = 0.25$ for the straggling, and $\alpha_0 = 1.5, 0.97$ and 0.8 for the inverse mean-free path of electrons, for the Lindhard, Levine-Louie and Brandt-Reinheimer models respectively. We notice that the limiting straggling value with $\alpha = 0.25$ yields a lower limit in the case of positrons (Fig. 2b panel (3)) and an upper limit in the case of electrons (Fig. 3b panel (3)). The first effect indicates an overshooting, similar to, but still larger than the one obtained for protons (Fig. 1b panel (3)). The second effect is a new one and shows a significant reduction of the straggling of electrons as a consequence of the identity of incident and target particles.

3.4 Comparative results

The results of the total energy loss moment calculations using the Lindhard and Levine-Louie dielectric models

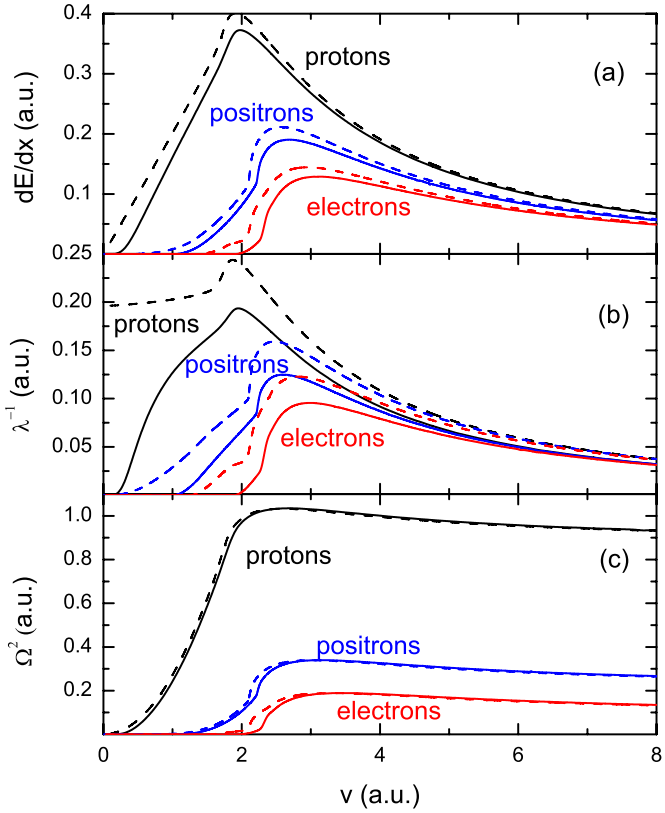

Fig. 4. Total contributions (individual + collective excitations) to the energy-loss moments versus the projectile velocity for different projectiles impinging on a medium represented by a free electron gas with $r_s = 1.5$ a.u. Comparisons between dielectric models: dashed-line, Lindhard model (energy gap = 0 eV); full-line, Levine-Louie model (energy gap = 14 eV); panel (a) stopping power vs. projectile velocity; panel (b) inverse mean-free-path vs projectile velocity; panel (c) straggling vs projectile velocity.

are shown in Figure 4 for the cases of protons, positrons and electrons traversing an electron gas characterized by $r_s = 1.5$. For the sake of clarity we include here only the calculations using the L and L-L models. Figure 4 shows that the most notorious differences appear for low energies, where the results are strongly reduced for all the projectiles when an energy gap is present. The contributions are also lower for positrons than for protons in all the cases, for the whole energy range. This latter result is a natural consequence of the restrictions imposed by the fact that the maximum energy transfer for positrons, $\varpi_{\max} = kv - \frac{k^2}{2m_e}$, is lower than for protons, where $\varpi_{\max} = kv - \frac{k^2}{2m_p}$, with $m_p = 1836 m_e$, which makes the quadratic term negligible in the case of protons.

Figure 4 also shows that the results for electrons are even lower than for positrons in all the cases. This is also caused by the additional restrictions to the maximum transferred energy in the case of electrons, indicated in Section 2, and by the effect of the exchange function $f_{ex}(k)$ in equations (2)–(4). As it has been observed in previous paragraphs, these new ingredients in the calculus arise as a consequence of the indistinguishability between the projectile and the target particles when the incident particle is an electron.

4 Conclusions

This work contains the first comparative study of the three main moments of the energy losses of protons, electrons and positrons using three dielectric models to represent the excitations of valence electrons in metals, semiconductors and insulators. We used for this purpose three dielectric models: the Lindhard model, appropriate for a free electron gas, and the Levine-Louie and Brandt-Reinheimer models which include the effects of band gaps in the excitation of individual electrons and collective modes. We described in detail the effects of band gaps in these materials, showing important changes in the contributions of individual and collective (plasmon) excitations to the stopping power, inelastic mean-free path, and energy straggling, for a wide range of energies, showing also characteristic features in each energy range and for each case. The low energy range is where the effects of the band gaps are stronger. They produce different threshold effects in all the energy loss moments and, in particular, great changes in the mean-free paths for all the particles here considered. At intermediate energies, we observe a displacement of the plasmon threshold in all cases, and a significant overshooting of the straggling of protons and positrons; the results for electrons are strongly affected by the restrictions imposed by the effects of particle indistiguishability and fermionic character (Pauli principle). The high (non-relativistic) energy limits show in all cases a simple behavior that can be described by simple asymptotic formulas which can be derived analytically using the plasmon-pole approximation. Finally, we included an Appendix where the integration of the plasmon resonance as well as the plasmon-pole approximation are briefly reviewed and the asymptotic limits of the energy loss moments are obtained.

On the basis of these results, and adding the effects of inner shell excitations, we will consider applications to specific semiconductors and insulator materials in a separate publication. We expect that the largest threshold effects could be observed in the case of high band-gap insulators such as those mentioned in Section 3, which would be among the most appropriate materials for studying that kind of effects, while much smaller effects may be expected for semiconductors. However, the main and strong differences between protons, electrons and positrons, should be present in all type of materials (metals, semiconductors and insulators) since those differences arise from the fundamental properties of each particle.

As a final consideration, we hope that this comparative study will be useful for applications in several cases of interest such as those mentioned at the beginning of this article.

Appendix

We consider here a method to integrate the plasmon contribution to the energy loss moments by transforming the doble integral into a line integral along the plasma resonance curve. We start with the expression for the energy-loss moments of a charge $Z_1 e$ in the form

$$Q_n = \frac{2}{\pi}\left(\frac{Z_1 e}{v}\right)^2 \hbar^{n-1}\int_0^{k_{\max}}\frac{dk}{k} \times \int_0^{\omega_{\max}} \omega^n \,\mathrm{Im}\left[\frac{-1}{\varepsilon(k,\omega)}\right] d\omega, \tag{A.1}$$

where we have set $f_{ex}(k) = 0$, so this calculation applies correctly to protons and positrons, and has only some restricted applicability in the case of electrons. This expression of Q_n yields the values of the mean-free-path, stopping power, and straggling when $n = 0, 1$ and 2 respectively. The units of Q_n are *(energy)^n/length*.

In the absence of damping effects, the plasmon resonance is described by a resonance line in the $k-\omega$ plane defined by the root of the equation $\varepsilon(k,\omega) = 0$. The solution of this equation provides a dispersion relation for plasmons that we shall call ω_k, which is a real function of k in the range $0 < k < k_c$, where the value of k_c is the point where the resonance line merges into the region of individual excitations, which opens a channel for plasmon decay [10,15] Hence, the range where plasmons are a well-defined collective mode is $0 < k < k_c$.

To transform the previous expression into a line integral we consider the following limit of the energy loss function in the region of the plasma resonance

$$\mathrm{Im}\left[\frac{-1}{\varepsilon(k,\omega)}\right] = \mathrm{Lim}\left[\frac{\varepsilon_2(k,\omega)}{\varepsilon_1(k,\omega)^2+\varepsilon_2(k,\omega)^2}\right]_{\varepsilon_2(k,\omega)\to 0} = \pi\delta\left[\varepsilon_1(k,\omega)\right] \tag{A.2}$$

and using the properties of the Dirac-delta function we get:

$$\mathrm{Im}\left[\frac{-1}{\varepsilon(k,\omega)}\right] = \frac{\pi}{D(k)}\delta(\omega-\omega_k) \tag{A.3}$$

where

$$D(k) = \left|\partial\varepsilon_1(k,\omega)/\partial\omega\right|_{\omega_k}. \tag{A.4}$$

Using this expression in the Q_n integral and limiting the k integral to the plasmon range we get

$$Q_n = \frac{2}{\pi}\left(\frac{Z_1 e}{v}\right)^2 \hbar^{n-1}\int_{k_{\min}}^{k_c}\frac{dk}{k}\frac{\pi\omega_k^n}{D(k)}. \tag{A.5}$$

This is an exact expression for the plasmon resonance contribution to the energy-loss moments for protons and positrons and yields a high-energy estimation in the case of electrons.

We consider now a simplified representation of the dielectric function of a free electron gas, which is usually called the plasmon-pole approximation (PPA) [16]

$$\varepsilon(k,\omega) \cong 1 - \frac{\omega_p^2}{\omega^2+\omega_p^2-\omega_k^2}. \tag{A.6}$$

Here ω_k is the plasmon frequency, which is determined from the condition $\varepsilon(k,\omega) = 0$. A numerical solution of this equation may be obtained using the particular models (Lindhard, BR or LL) described before. Alternatively, useful analytical approximations have been provided in the context of the PPA by previous authors [6,7,16,17]

$$\omega_k^2 \cong \omega_p^2 + E_g^2/\hbar^2 + \beta^2 k^2 + \gamma^2 k^4 \tag{A.7}$$

where β is a typical velocity, related to the Fermi speed as $\beta^2 = (3/5)v_F^2$ and $\gamma = \hbar/2m$.

Using the previous expression of $\varepsilon(k,\omega)$ one gets $D(k) = 2\omega_k/\omega_p^2$, and therefore

$$Q_n \approx \left(\frac{Z_1 e}{v}\right)^2 \hbar^{n-1}\omega_p^2\int_{k_{\min}}^{k_{\max}}\frac{dk}{k}\omega_k^{n-1} \tag{A.8}$$

where the values of $k_{\min}$ and $k_{\max}$ are defined below. This is a general expression for the energy loss moments in the context of the PPA. Notice that the upper limit of the integral has been extended to $k_{\max}$. This is consistent with the PPA since the aim of this approximation is to extend the domain of integration so as to include both collective and individual excitations in an approximate way [16]. We also notice that while equation (A.5) applies exactly to the plasmon resonance, equation (A.8) aims at describing both plasmon and single-particle excitations in an approximate way.

Several useful approximations can be derived from this expression. For instance, for $n = 1$ we retrieve the well-known Bethe expression for the high-energy stopping power:

$$\frac{dE}{dx} = Q_1 \approx \left(\frac{Z_1 e\omega_p}{v}\right)^2 \ln\left(\frac{k_{\max}}{k_{\min}}\right) \approx \left(\frac{Z_1 e\omega_p}{v}\right)^2 \ln\left(\frac{\alpha_1 m v^2}{\hbar\overline{\omega}_p}\right), \tag{A.9}$$

where $\overline{\omega}_p = \left[\omega_p^2 + E_g^2/\hbar^2\right]^{1/2}$.

For $n = 0$ we get a similar expression for the inverse mean-free path

$$\lambda^{-1} = Q_0 \approx \left(\frac{Z_1 e}{v}\right)^2 \frac{\omega_p^2}{\hbar\overline{\omega}_p}\ln\left(\frac{k_c v}{\overline{\omega}_p}\right) \approx \left(\frac{Z_1 e}{v}\right)^2 \frac{\omega_p^2}{\hbar\overline{\omega}_p}\ln\left(\alpha_0\frac{v}{v_F}\right), \tag{A.10}$$

and for $n = 2$ we get the high-energy result for the straggling

$$\Omega^2/dx = Q_2 \approx (Z_1 e\omega_p)^2 m\left(\frac{\hbar k_{\max}}{2mv}\right)^2 \approx \alpha_2 m (Z_1 e\omega_p)^2. \tag{A.11}$$

In these expressions the value of $k_{\min}$ is given by $\overline{\omega}_p/v$ (high-energy limit), whereas the value of $k_{\max}$ depends on the particle being considered, namely: $k_{\max} = \alpha_1 mv$, with $\alpha_1 = 2$ for protons and 1 for positrons. These values

correspond to the largest momentum transfer in the high-energy limit. In the case of electrons, the condition that the maximum energy transfer does not exceed the value $T/2$ yields $\alpha_1 = \sqrt{2}$; additionally, in this case the correction term $f_{ex}(k)$ must be considered, and so the value of α_1 differs from the previous ones.

To obtain the corresponding approximation for the inverse mean-free path λ^{-1}, it should be noticed that the term ω_k^{-1} in equation (A.8) is nearly constant ($\omega_k \sim \overline{\omega}_p$) for $k < k_c$ and it drops very rapidly for k larger than k_c, so that the upper limit in this integral can be approximated by $k_c \sim \alpha_0 \omega_p / v_F$, where the value of α_0 is determined numerically.

On the other hand, when calculating the straggling integral, the factor ω_k in equation (A.8) produces a large contribution of the highest k values (binary collision limit); therefore, by approximating $\omega_k \sim \gamma k^2$ (last term in Eq. (A.7)) we obtain the result of equation (A.11) with $\alpha_2 = \alpha_1^2/4$ (i.e., $\alpha_2 = 1$ and $1/4$ for protons and positrons respectively).

These expressions are useful to explain the high-energy limits of the results shown in the various figures of this paper.

C.D. Archubi is a research staff member of CONICET, Argentina. The authors acknowledge support from Universidad Nacional de Cuyo and ANPCYT, Argentina.

References

1. J.C. Ashley, C.J. Tung, R.H. Ritchie, Surf. Sci. **81**, 409 (1979)
2. A. Akkermann et al., Phys. Stat. Sol. B **198**, 769 (1996)
3. J.M. Fernández-Varea, R. Mayol, D Liljequist, F. Salvat, J. Phys.: Condens. Matter **5**, 3593 (1993)
4. A. Jablonsky, C.J. Powell, Surf. Sci. Rep. **47**, 33 (2002)
5. J. Lindhard, K. Dan, Vidensk. Selsk., Mat.-Fys. Medd. **28**, 1 (1954)
6. W. Brandt, J. Reinheimer, Phys. Rev. B **2**, 3104 (1970)
7. W. Brandt, J. Reinheimer, Phys. Rev. B **4**, 1395 (1971)
8. Z.H. Levine, S.G. Louie, Phys. Rev. B **25**, 6310 (1982)
9. C.D. Archubi, N.R. Arista, Eur. Phys. J. B **89**, 86 (2016)
10. J. Lindhard, A. Winther, K. Dan. Vidensk. Selsk., Mat.-Fys. Medd. **34**, 1 (1964)
11. R. García-Molina, I. Abril, I. Kyriakou, D. Emfietzoglou, *Surface and Interface Analysis* (Wiley Online Library, 2016)
12. C.E. Celedón, G.H. Lantschner, N.R. Arista, Nucl. Instrum. Methods B **315**, 21 (2013)
13. E. Bonderup, P. Hvelplund, Phys. Rev. A **4**, 562 (1971)
14. R.H. Ritchie, Phys. Rev. **114**, 644 (1959)
15. D. Pines, *Elementary Excitations in Solids* (W.A. Benjamin Inc., New York, 1964)
16. R.H. Ritchie, W. Brandt, P.M. Echenique, Phys. Rev. B **14**, 4808 (1976)
17. P.M. Echenique, R.H. Ritchie, W. Brandt, Phys. Rev. B **20**, 2567 (1979)